


ARTICLE



Leukemia/lymphoma-related factor (LRF) or osteoclast zinc finger protein (OCZF) overexpression promotes osteoclast survival by increasing *Bcl-xl* mRNA: A novel regulatory mechanism mediated by the RNA binding protein SAM68

Xianghe Xu^{1,2,6}, Takeo Shobuike¹, Makoto Shiraki³, Asana Kamohara⁴, Hirohito Hirata³, Masatoshi Murayama³, Daisuke Mawatari³, Masaya Ueno³, Tadatsugu Morimoto³, Toshio Kukita², Masaaki Mawatari³ and Akiko Kukita^{1,5} 

© The Author(s), under exclusive licence to United States and Canadian Academy of Pathology 2022

RANKL induces NFATc1, a key transcriptional factor to induce osteoclast-specific genes such as cathepsin K, whereas transcriptional control of osteoclast survival is not fully understood. Leukemia/lymphoma-related factor (LRF) in mouse and osteoclast zinc finger protein (OCZF) in rat are zinc finger and BTB domain-containing protein (ZBTB) family of transcriptional regulators, and are critical regulators of hematopoiesis. We have previously shown that differentiation and survival were enhanced in osteoclasts from OCZF-Transgenic (Tg) mice. In the present study, we show a possible mechanism of osteoclast survival regulated by LRF/OCZF and the role of OCZF overexpression in pathological bone loss. In the in vitro cultures, LRF was highly colocalized with NFATc1 in cells of early stage in osteoclastogenesis, but only LRF expression persisted after differentiation into mature osteoclasts. LRF expression was further enhanced in resorbing osteoclasts formed on dentin slices. Osteoclast survival inhibitor such as alendronate, a bisphosphonate reduced LRF expression. Micro CT evaluation revealed that femurs of OCZF-Tg mice showed significantly lower bone volume compared to that of WT mice. Furthermore, OCZF overexpression markedly promoted bone loss in ovariectomy-induced osteolytic mouse model. The expression of anti-apoptotic *Bcl-xl* mRNA, which is formed by alternative splicing, was enhanced in the cultures in which osteoclasts are formed from OCZF-Tg mice. In contrast, the expression of pro-apoptotic *Bcl-xs* mRNA was lost in the culture derived from OCZF-Tg mice. We found that the expression levels of RNA binding splicing regulator, Src substrate associated in mitosis of 68 kDa (Sam68) protein were markedly decreased in OCZF-Tg mice-derived osteoclasts. In addition, shRNA-mediated knockdown of Sam68 expression increased the expression of *Bcl-xl* mRNA, suggesting that SAM68 regulates the expression of *Bcl-xl*. These results indicate that OCZF overexpression reduces protein levels of Sam68, thereby promotes osteoclast survival, and suggest that LRF/OCZF is a promising target for regulating pathological bone loss.

Laboratory Investigation (2022) 102:1000–1010; <https://doi.org/10.1038/s41374-022-00792-w>

INTRODUCTION

Leukemia/lymphoma-related factor (LRF) in mouse and osteoclast zinc finger protein (OCZF) in rat are members of the ZBTB family of protein also known as ZBTB7A. LRF is a pleiotropic transcriptional regulator and has been characterized as an oncogene in human cancers^{1,2}. ZBTB7A overexpression is associated with tumor progression which promotes cell survival, proliferation, and metastasis in lymphoma, breast, lung, liver, and colon cancer^{3,4}. However, ZBTB7A also suppresses tumor growth of some types of prostate cancer cells⁵. On the other hand, LRF has been shown to be a critical regulator of differentiation and commitment of hematopoietic and lymphoid cells^{6,7}. LRF acts as a regulator in the lineage commitment to B cells and the differentiation into

regulatory T cells^{8,9}. In addition to the differentiation process of early progenitors, LRF plays role in terminally differentiated cells. LRF is highly expressed in germinal B cells and regulates mature B cell fate by regulating proliferation and survival¹⁰. LRF is induced by GATA1 and inhibits apoptosis of terminal differentiated erythrocytes by regulating Bim¹¹.

ZBTB family proteins have two conserved domains, the N-terminal broad complex/tram-track/bric-a-branc (BTB) domain and C-terminal zinc finger motifs which bind to DNA. BTB domain is responsible for dimerization of LRF and interaction with various corepressors and transcriptional factors¹. LRF forms homodimer or heterodimers with BCL6, and recruits transcription corepressors such as NCOR and SMRT via BTB domain¹. In addition, BTB domain

¹Department of Pathology and Microbiology, Faculty of Medicine, Saga University, Saga, Japan. ²Department of Molecular Cell Biology & Oral Anatomy, Faculty of Dentistry, Kyushu University, Fukuoka, Japan. ³Department of Orthopaedic Surgery, Faculty of Medicine, Saga University, Saga, Japan. ⁴Department of Oral & Maxillofacial Surgery, Faculty of Medicine, Saga University, Saga, Japan. ⁵Research Center of Arthroplasty, Faculty of Medicine, Saga University, Saga, Japan. ⁶Present address: Department of Orthopaedics, The Fifth Affiliated Hospital of Sun Yat-sen University, Zhuhai 519000 Guangdong, China. [✉]email: kukita@cc.saga-u.ac.jp

Received: 5 November 2021 Revised: 8 April 2022 Accepted: 11 April 2022

Published online: 26 April 2022

Table 1. List of primers used for RT-qPCR analysis.

	Sense	Anti-sense
<i>Lrf</i>	5'-GAGAAGAAAATCCGGGCCAAG -3'	5'- GCAGCTATCGCACTGGTATGG -3'
<i>Ctsk</i>	5'-CTCTCGGCGTTTAATTTGGGAG -3'	5'-CCCTGGTTCTTGACTGGAGTAACG -3'
<i>Sam68</i>	5'-GTGGAGACCCCAAATATGCCCA -3'	5'-AAACTGCTCCTGACAGATATCA -3'
<i>Bcl-xl</i>	5'-GCTGGGACACTTTTGTGGAT -3'	5'-TGCTGGTCACTTCCGACTG -3'
<i>Bim</i>	5'-CGACAGTCTCAGGAGGAACC -3'	5'-CCTTCTCCATACCAGACGGA -3'
<i>Gapdh</i>	5'-TGCACCACCAACTGCTTAG-3'	5'-GGATGCAGGGATGATGTC-3'

serves as the “adaptor” for ubiquitination by binding E3 ubiquitin ligase CULLIN3 (CUL3). Interaction of ZBTB family proteins PLZF and BCL-6 with CUL3 modulates lymphocyte development and function^{12,13}. Amino acids sequences of mouse, rat, and human orthologues of ZBTB7A are highly conserved, and 98–100% similarities are detected in BTB region and zinc finger motifs.

Osteoclasts are derived from hematopoietic stem cells, and are differentiated from cells of the monocyte/macrophage lineage. Receptor activator of NF- κ B ligand (RANKL) and macrophage colony-stimulating factor (M-CSF) are essential factors for osteoclast differentiation. Terminally differentiated osteoclasts are cell-cycle arrested multinucleated cells. Osteoclasts are then activated on bone matrix components by integrin-mediated signals. Activated osteoclasts have a short life span. After the osteoclast have completed resorbing bone, osteoclasts undergo apoptosis. Osteoclasts formed in vitro bone marrow culture die by apoptosis in the absence of cytokines. Cytokines including M-CSF, RANKL, IL-1 β , TNF α , and lipopolysaccharide (LPS) enhanced survival of osteoclasts formed in culture^{14,15}. It is known that death receptor pathway and mitochondria pathway including Bcl-2 family proteins regulate osteoclast apoptosis^{16–18}. Bisphosphonates down-regulate osteoclast activity and induce osteoclast apoptosis¹⁹. TNF- α inhibited bisphosphonates-induced apoptosis by enhancing anti-apoptotic Bcl-xl expression²⁰. Loss of estrogen causes osteoporosis in postmenopausal women. Estrogen directly stimulated osteoclast apoptosis by inducing Fas ligand expression in osteoclasts²¹, while estrogen stimulated apoptosis of osteoclast precursors by promoting Bak and Bax-dependent mitochondria pathway²². Estrogen deficiency influences immune cells to increase the production of pro-inflammatory cytokines²³. These reports suggest that osteoclast survival is involved in pathological bone loss.

We have shown that LRF plays stage-specific roles in osteoclastogenesis by analyzing mice that lack LRF gene in the different stages of osteoclastogenesis²⁴. Mx1-Cre mediated LRF deletion in the early stage of osteoclastogenesis decreased bone volume, whereas Ctsk-Cre mediated LRF deletion in the late stage of osteoclastogenesis increased bone mass. The analysis of bone phenotypes of these mice indicated that LRF inhibits early osteoclastogenesis, but stimulates bone resorption in mature osteoclasts. We have also prepared OCZF transgenic (OCZF-Tg) mice which overexpress OCZF under the control of the cathepsin K promoter²⁵. OCZF-Tg mice exhibited osteoporotic phenotypes. Histomorphometric analysis of femurs showed that osteoclast number was increased, whereas osteoblast number was not changed. In vitro cultures of bone marrow cells from mice showed that osteoclastogenesis was enhanced in OCZF-Tg mice. Additionally, osteoclasts formed from OCZF-Tg mice have survived for a longer period of time after withdraw of RANKL and M-CSF, suggesting a role of LRF in osteoclast survival. However, the mechanism by which LRF promotes osteoclast survival remains unclear.

Previous study reported that FBI-1, the human orthologue of LRF/OCZF, regulates *Bcl-x* alternative splicing in prostate cancer cells²⁶. FBI-1 interacts with a RNA-binding splicing regulator Sam68, and inhibits the interaction of Sam68 with pro-apoptotic

Bcl-xs mRNA. Inhibition of Sam68-mediated *Bcl-xs* alternative splicing by FBI-1 leads to increased alternative splicing of anti-apoptotic *Bcl-xl* mRNA, which promotes cell survival²⁷. Sam68 was originally identified as a target of activated Src in fibroblasts²⁸, and now recognized as an important RNA binding protein that regulates alternative splicing of several genes^{27,29}. In the present study, we investigated the role of LRF/OCZF in ovariectomy-induced bone loss. We have further investigated whether *Bcl-xl* alternative splicing by Sam68 is involved in the modulatory mechanism of LRF/OCZF in osteoclast survival.

MATERIALS AND METHODS

Reagents and chemicals

FBS was purchased from Gibco (Grand Island, NY). Recombinant human soluble RANKL, M-CSF, IL-1 β , and IL-6 were purchased from Pepro-Tech (Rocky Hill, NJ). TNF- α was purchased from R&D Systems (Minneapolis, MN). LPS from *Escherichia coli* O55:B5 was purchased from Sigma-Aldrich (St. Louis, MO, USA). Rabbit anti-OCZF polyclonal IgG produced by immunizing the animals with purified recombinant OCZF-GST fusion protein was used as described²⁵. Anti-GAPDH (sc-25778) rabbit antibody, anti-cathepsin K (sc-48353), anti-nuclear factor of activated T cell 1 (NFATc1) (sc-7294), and anti-Sam68 (sc-1238) mouse antibodies were obtained from Santa Cruz Biotechnology (Santa Cruz, CA). LY294002 (L-7962), a phosphatidylinositol-3 kinase (PI3K) inhibitor, and Dasatinib (D-3307), a Src inhibitor were obtained from LC Laboratories (Woburn, MA). Alendronate was obtained from Calbiochem (San Diego, CA). The tartrate-resistant acid phosphate (TRAP) assay kit was obtained from Sigma-Aldrich.

Mice and rats

OCZF Tg (C57BL/6) mice (aged 7–12 weeks) expressing OCZF and EGFP fusion protein under the control of 1.6 kb cathepsin K promoter was used as described²⁵. OCZF transgene-negative littermates were used as wild-type (WT) mice. Lewis rats were obtained from Kyudo (Tosu, Saga, Japan). All mice and rats were housed under pathogen-free conditions and fed standard rodent diet. All experiments were carried out according to the protocol approved by the Laboratory Animal Care and Use Committee of Saga University and Kyushu University.

Cell culture for osteoclastogenesis

Mouse bone marrow culture was performed as described previously²⁵. Briefly, nonadherent bone marrow cells were isolated from female or male mice, and nonadherent bone marrow cells were cultured in α -MEM containing 15% FBS in the presence of M-CSF (10 ng/ml) for 3 days to generate bone marrow macrophages (BMMs). Osteoclasts were differentiated from BMMs with RANKL (50 ng/ml) and M-CSF (10 ng/ml) for 2–3 days. In some experiments, BMMs stimulated with RANKL for 24 h were detached from the culture plate by 0.05% trypsin and 0.01% EDTA, and then re-seeded on dentin slices to form osteoclasts as described³⁰. The cells were cultured on dentin slices in the presence of RANKL (50 ng/ml) and M-CSF (10 ng/ml) for an additional 36–48 h. At the end of the culture, the cells were lysed for protein and RNA analysis or fixed for immunostaining.

RT-quantitative PCR (RT-qPCR) and RT-PCR

Total RNA was extracted using RNA Isoplus (Takara Bio, Shiga, Japan). cDNA was synthesized using random primers with ReverTra Ace qPCR RT Master Mix (Toyobo, Osaka, Japan). Primers for RT-qPCR are listed in Table 1. Quantitative real-time PCR was performed using THUNDERBIRD SYBR qPCR

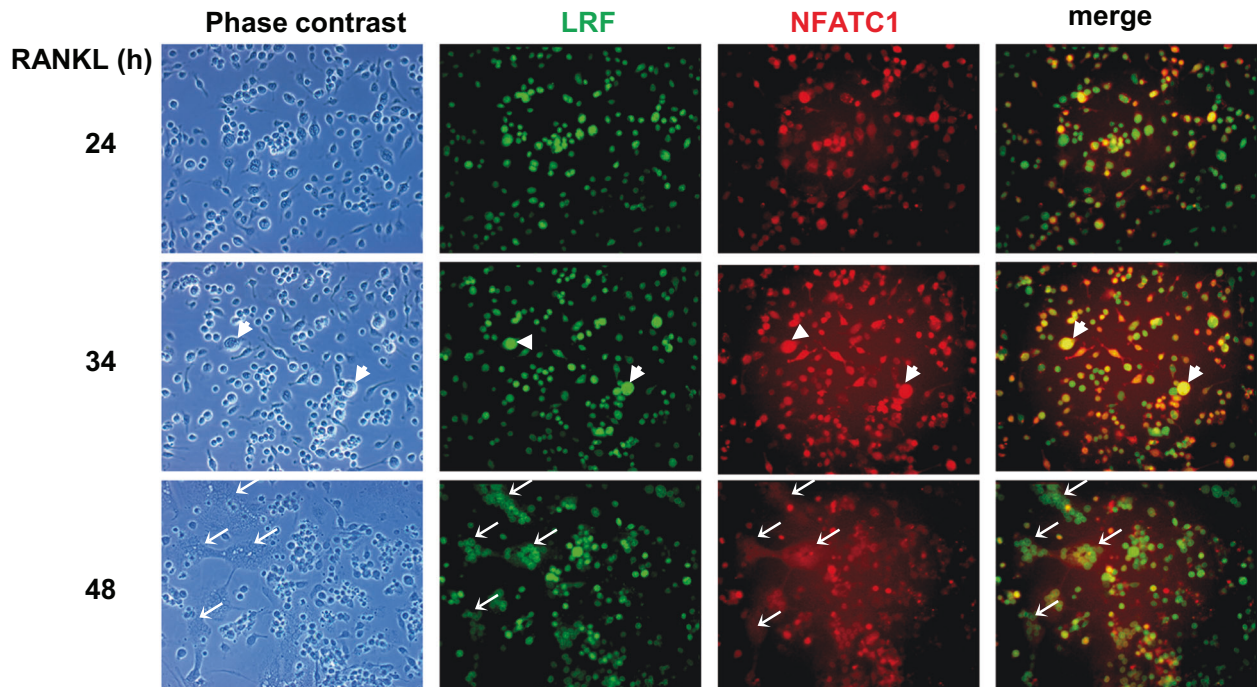


Fig. 1 Immunofluorescence colocalization of LRF and NFATc1 in osteoclastogenesis. BMMs were cultured in the presence of M-CSF (10 ng/ml) and RANKL (50 ng/ml) for the indicated times. After culturing, cells were fixed, and immunostained for LRF (green) and NFATc1 (red). Phase contrast images are also shown in the left panels. Merged fluorescence images are shown in the right panels. Arrow heads indicate small osteoclasts at 34 h stained with LRF and NFATc1. Arrows indicate large osteoclasts at 48 h stained with LRF but not with NFATc1.

Mix (Toyobo) with a Step One plus real-time PCR system (Applied Biosystems, Foster City, CA). mRNA levels were normalized to *Gapdh* expression. In some experiments, PCR was performed using Ex Taq (Takara Bio). PCR products were separated on a 1.5% agarose gel and stained with ethidium bromide. Reactions were conducted in a 10 μ l reaction mixture and were incubated for 1 min at 94 $^{\circ}$ C, followed by 45–50 cycles of a three-step amplification procedure composed of annealing for 30 s at 55 $^{\circ}$ C, extension for 1 min at 72 $^{\circ}$ C, and denaturation for 30 s at 94 $^{\circ}$ C. The following primers were used to amplify both *Bcl-xl* and *Bcl-xs* mRNAs: mouse *Bcl2l1* (*Bcl-x* NM_001289716), sense, 5'-GCTGGAGTCAGTTTAGTGATG-3', antisense, 5'-TCACTCCGACTGAA GAGTG-3'. PCR reactions generated a 615 bp product from *Bcl-xl* mRNA and a 426 bp product from *Bcl-xs* mRNA.

Western blot analysis

To isolate cell extracts, the cells were washed with PBS and the cells were lysed in RIPA buffer (25 mM Tris-HCl, pH 7.4, 5 mM EDTA, 150 mM NaCl, 1% Triton, 2.5 mM sodium pyrophosphate, 0.7 mM β -glycerophosphate) supplemented with protease inhibitor cocktail (Sigma) and phosphatase inhibitor cocktail 2 (Sigma) for 30 min on ice. Insoluble material was removed by centrifugation at 12,000 $\times g$ for 5 min at 4 $^{\circ}$ C. Supernatants were collected. Protein concentration was measured using a BCA protein assay kit (Thermo Fisher Scientific, Waltham, MA). Equal amounts of proteins were separated by 10% SDS-PAGE and transferred to polyvinylidene fluoride membranes (Bio Rad, Hercules, CA). The membranes were blocked with 5% skim milk in TBS containing 0.1% Tween-20 at room temperature (20–25 $^{\circ}$ C) for 1 h. Blots were incubated with primary antibodies at room temperature for 1 h. HRP-conjugated anti-rabbit (7074, Cell Signaling Technology, Danvers, MA) or anti-mouse antibodies (sc-516102, Santa Cruz Biotechnology) were used as secondary antibodies. The membranes were incubated with secondary antibodies for 1 h at room temperature. Antibody detection was performed with ECL Prime Western Blotting Detection Reagent (GE Healthcare, Little Chalfont, UK). Blots were visualized using the LAS-4000 image analyzer (Fujifilm, Tokyo, Japan).

Immunofluorescence staining of cultured cells

For staining with anti-OCZF and anti-NFATc1 antibodies, cells were fixed in 99:3 cold methanol/formaldehyde for 20 min at -20° C, permeabilized in 0.2% Triton X-100 for 10 min at room temperature. For staining with anti-Sam68 antibody, cells were fixed with 4% paraformaldehyde (PFA) for 20 min. The

fixed cells were blocked by incubation in 3% normal goat serum for 60 min at room temperature. The cells were then incubated with rabbit anti-OCZF, mouse anti-NFATc1, or mouse Sam68 antibodies for 60 min. The cells were washed and then incubated with secondary antibodies. Microscopic observations were performed using fluorescence microscope (Zeiss) or LSM5 PASCAL confocal laser microscope (Carl Zeiss). To examine the cells on dentin, dentin slices were placed upside down on a glass bottom dish and examined from beneath the dish.

Construction of plasmids

Lentivirus shRNA plasmids were constructed as described using pRSI9-U6-sh-UbiC-RFP-2A-Puro (addgene # 28289)³¹. The sense strand sequences of the shRNA specifically targeting *Sam68* mRNA were 5'-CCAAGATTCTTAC-GAAGCCTA-3'. As a control, a previously reported shRNA targeting the mRNA of *Egfp* with the sense strand sequence 5'-CGGCATCAAGGT-GAACTCAA-3' was used³¹.

Lentivirus production and infection of osteoclasts

Recombinant lentiviruses were produced by transfecting 293T cells with the lentivirus plasmid, packaging plasmid psPAX2 (addgene #12260), and envelope plasmid pMD2.G (addgene #12259) as described³¹. The culture medium containing viruses was harvested at 48 h after transfection and concentrated by centrifugation at 14,000 rpm for 1 h at 4 $^{\circ}$ C. Viral titers were determined by MACS Quant Analysis (Miltenyi Biotec.) for RFP expression. For infection of osteoclasts, BMMs stimulated with RANKL (50 ng/ml) for 48 h were transduced with shRNA lentiviruses (Moi=10) for 12 h. The cells were stimulated with RANKL (50 ng/ml) for another 36 h.

Induction of adjuvant arthritis in rats and immunofluorescence staining

Adjuvant arthritis was induced as described previously³². Briefly, 5-week-old female Lewis rats were anesthetized with isoflurane inhalation and were intradermally injected at the base of the tail with complete Freund adjuvant containing 25 mg/kg heat-killed *M. butyrium* (Difco Laboratories, Detroit, MI) suspended in mineral oil. The rats were killed on day 21 after injection. After anesthetizing with isoflurane inhalation followed by intraperitoneal injection of pentobarbital (1 mg/kg body weight), the rats were aseptically dissected and fixed by perfusion 4% PFA from the left

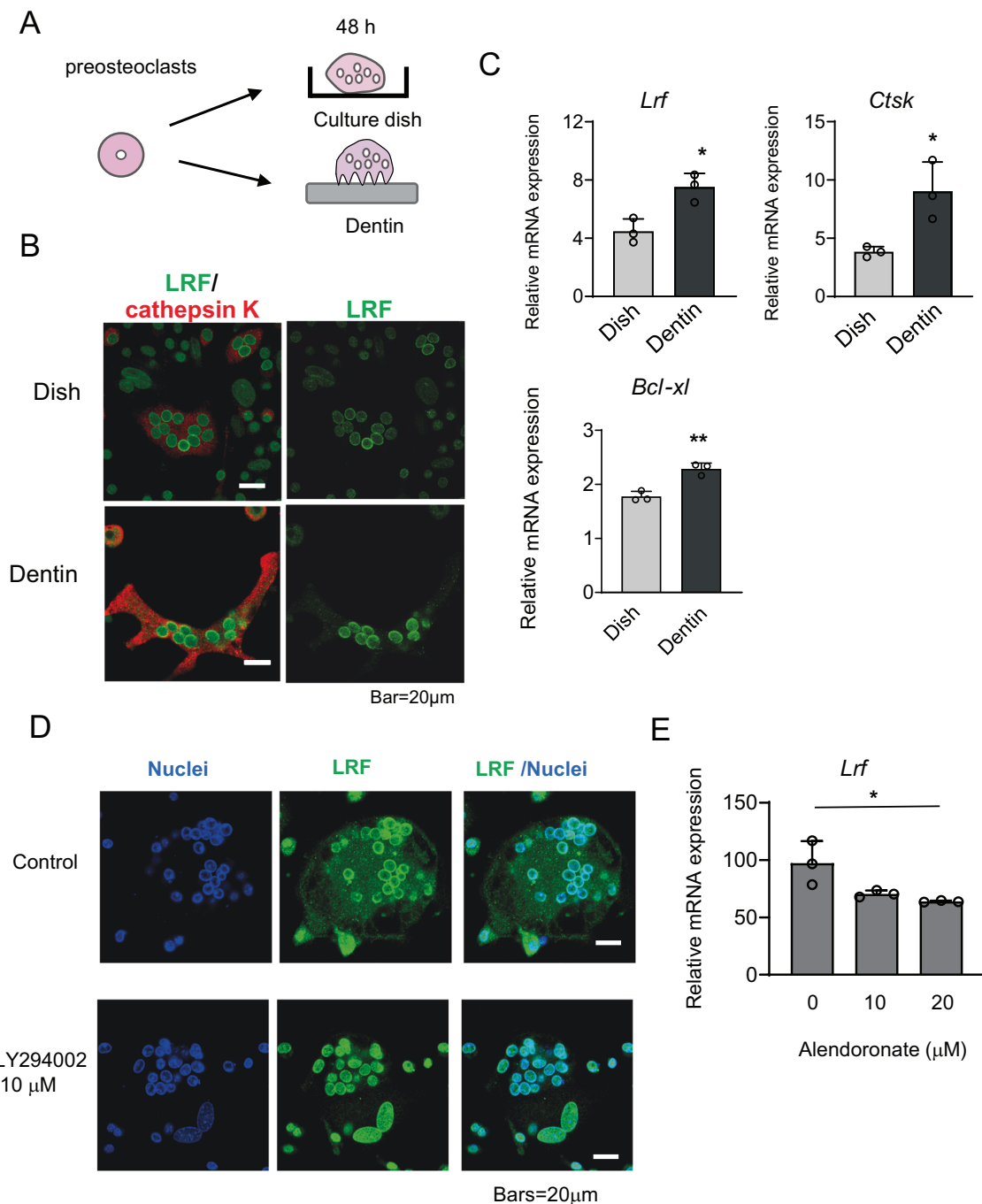


Fig. 2 LRF expression is associated with osteoclast survival. **A** Diagram of experimental setup. BMMs were incubated with M-CSF (10 ng/ml) and RANKL (50 ng/ml) for 48 h. Cells were detached, re-seeded in culture dishes or dentin slices, and cultured for another 48 h. **B** Immunofluorescence staining of osteoclasts formed on culture dishes or dentin slices with LRF and cathepsin K antibodies. Bar = 20 μm. After culturing, cells were fixed, and stained for LRF (green) and cathepsin K (red). **C** RT-qPCR analysis of *Lrf*, *Ctsk*, or *Bcl-xl* expression in the cells formed on culture dishes or dentin slices. **D** 10 μM LY294002 was added to osteoclasts for 12 h. After culturing, cells were fixed, and stained for LRF (green). Nuclei were stained with To-Pro-3 iodide (blue). **E** After 48 h of BMMs stimulated with RANKL, alendronate was added for 24 h. RT-qPCR analysis of *Lrf* expression in osteoclasts was performed. In RT-qPCR analysis, expression was normalized with *Gapdh* ($n = 3$). Data are presented as mean \pm SD. Student's *t*-test was used for statistical analysis in **C**. * $P < 0.05$, ** $P < 0.01$ compared to osteoclasts formed on culture dishes (**C**). The differences between means and effects of treatments were determined by one-way ANOVA followed by Tukey's post hoc test in (**E**). * $P < 0.05$, compared to osteoclasts cultured without alendronate (**E**).

ventricle. Ankle joints were isolated and immersed in the same fixative for overnight at 4 °C, followed by washing in PBS. After decalcification in 10% EDTA for 3 weeks at 4 °C, tissue blocks were embedded in OCT compound. Frozen sections were prepared and then processed for immunofluorescence analysis. After quenching unreacted aldehyde groups with 10 mM glycine, sections were blocked in 10% chick albumin for 60 min at room

temperature, followed by further blocking in 3% normal goat serum for 2 h at room temperature. Sections were then incubated with anti-cathepsin K and anti-OCZF antibodies at room temperature for 1 h. After washing, sections were incubated with secondary antibodies for 30 min. Microscopic observations were performed using an C2si confocal laser microscope (Nikon Instec, Tokyo, Japan)

Ovariectomy and micro-computed tomography

OCZF-Tg female mice and their wild-type counterparts were either ovariectomized (OVX) or sham-operated at 8 weeks of age, and subjected to micro-computed tomography (μ CT) analyses 4 weeks after surgery. The bone structure of femurs from 12-week-old mice was analyzed by μ CT as described³³. Femurs were dissected, cleaned of muscle and connective tissues, fixed in 4% PFA overnight at 4°C, and then stored in 70% ethanol. Femurs were scanned using the SkyScan-1076 X-ray micro-computed tomograph at 9 μ m pixel size, X-ray tube voltage of 48 kV, 1550 ms exposure time, and 200 μ A source current. Data series were reconstructed using SkyScan NRecon software and analyzed with SkyScan CT Analyzer (CTAn) software (Bruker, Billerica, MA). Trabecular bone was analyzed in the proximal metaphysis region, 0.9–3.5 mm above the distal growth plate of the femur, starting 100 slices proximal to the growth plate for 400 slices, each 9 μ m thick. Cortical bone was analyzed by the central diaphysis regions corresponding to 450 slice. Trabecular and cortical morphometric parameters were analyzed with adaptive threshold procedure using CTAn software (SkyScan), and quoted using American Society for Bone and Mineral Research nomenclature.

Statistical analysis

Data are presented as the means \pm SD. Comparison of data from two unpaired groups was performed using Student's *t*-test. To compare more than two groups, data were analyzed using one-way analysis of variance (ANOVA) followed by Tukey's post hoc test. *P*-values of less than 0.05 were considered statistically significant. Data shown are representative results from two or three independent experiments.

RESULTS

Intracellular colocalization analysis of LRF with NFATc1 in osteoclastogenesis

To know the role of LRF in osteoclastogenesis in details, we performed double-immunofluorescence staining analysis of LRF with NFATc1 in BMMs stimulated with RANKL. After 24–34 h of RANKL addition, LRF protein was appeared in preosteoclasts and small osteoclasts containing 2 or 3 nuclei which are also stained for NFATc1 (Fig. 1). After 48 h of culture, LRF was detected in nuclei of large osteoclasts, whereas NFATc1 expression was decreased in nuclei of several osteoclasts (Fig. 1). The results show that unlike NFATc1, LRF expression is sustained after differentiation into mature osteoclasts.

LRF expression is associated with osteoclast survival

Adhesion of osteoclasts to bone matrix components induces terminal differentiation of osteoclasts mediated by integrin

signaling³⁴. We then analyzed the expression of LRF in osteoclasts formed in culture dishes and those formed on dentin slices (Fig. 2A). Immunostaining signals of LRF and cathepsin K protein appeared to be stronger in osteoclasts formed on dentin slices than those in osteoclasts formed on culture dishes (Fig. 2B). In addition, LRF protein was detected in nuclei of both osteoclasts formed on dentin slices and those formed in culture dishes, but small dot-like signals were detected only in the cytoplasm of osteoclasts formed on dentin slices. RT-qPCR analysis showed that the expression of *Lrf* and *Ctsk* (cathepsin K) mRNA was significantly enhanced in the cells formed on dentin slices (Fig. 2C). We then analyzed the expression of anti-apoptotic *Bcl-xl* mRNA in osteoclasts. Expression of *Bcl-xl* mRNA was increased in the cells formed on dentin slices compared to those formed on culture dishes (Fig. 2C). Because the cells formed on dentin slices are mainly composed of osteoclasts, the results suggest that survival is enhanced in osteoclasts on dentin slices. Additionally, treatment of osteoclasts with 10 nM Dasatinib, a Src kinase inhibitor for 12 h changed the nuclear localization of LRF to diffuse cytoplasmic localization in osteoclasts on dentin slices (Supplemental Fig. 1), suggesting that integrin signaling may be involved in regulation of LRF expression. Addition of LY294002, a specific inhibitor of PI3K pathway which is involved in osteoclast survival³⁵, decreased cytoplasmic signals of LRF in osteoclasts (Fig. 2D). Furthermore, alendronate, a bisphosphonate that induces osteoclast apoptosis³⁶ decreased LRF expression in the cells in the osteoclast-lineage on dentin slices in a dose-dependent manner (Fig. 2E). These results strongly suggest that LRF expression is associated with osteoclast survival.

Expression of LRF/OCZF protein in osteoclasts at bone destruction area of arthritis rats

To evaluate the expression of LRF/OCZF protein in active osteoclasts in vivo, we analyzed LRF/OCZF expression in osteoclasts in bone destruction site of rats with adjuvant-induced arthritis by immunostaining. In this model, a number of osteoclasts are detected on bone destruction area of ankle joints of arthritis rats. As shown in Fig. 3, specific expression of LRF/OCZF protein was detected in nuclei of mature osteoclasts on bone, which highly express cathepsin K. Inflammatory cytokines and LPS have been shown to promote osteoclast survival^{14,15}. We found that TNF- α increased LRF expression in BMMs two fold, while IL-1 β , IL-6, and LPS markedly upregulated LRF expression in BMMs (Supplemental Fig. 2), suggesting that LRF/OCZF expression is enhanced under inflammatory conditions.

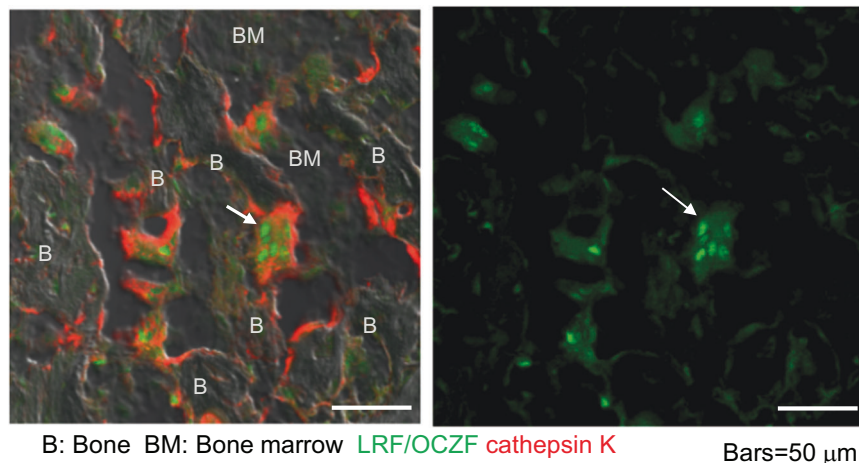


Fig. 3 LRF/OCZF protein was detected in osteoclasts expressing cathepsin K at bone destruction sites of adjuvant-induced arthritis rats. Immunofluorescence staining of osteoclasts in bone destruction sites of arthritic rats. Cryosections of ankle joints were incubated with rabbit anti-OCZF and mouse anti-cathepsin K antibodies, followed by detection with secondary antibodies. Arrow indicates typical osteoclasts containing three or more nuclei on bone. LRF/OCZF, green; cathepsin K, red; bone marrow, BM; Bone, B; scale bar = 50 μ m.

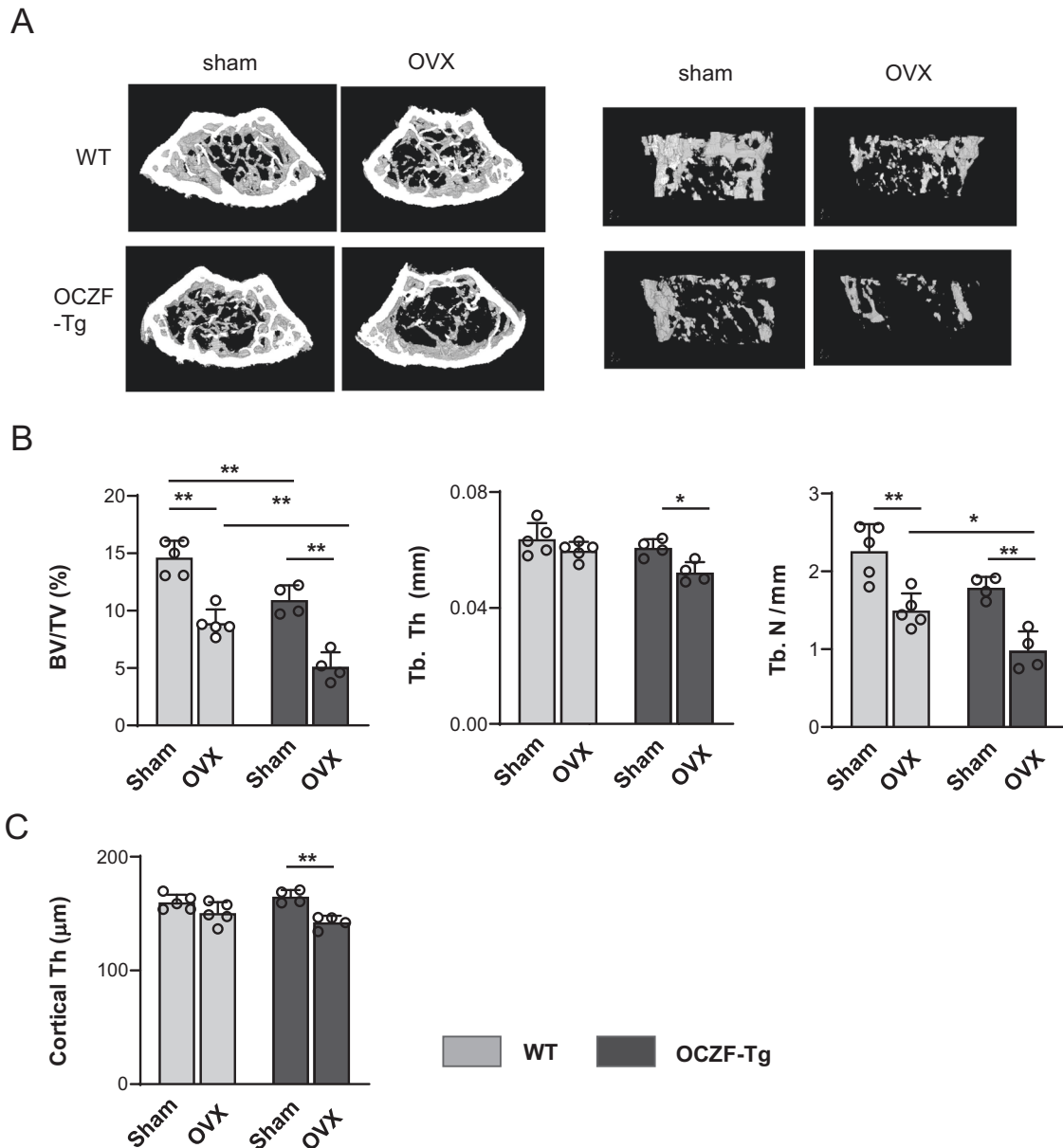


Fig. 4 OVX-induced bone loss was enhanced in OCZF-Tg mice. **A** μ CT images of the distal femurs of WT and OCZF-Tg female mice (12-week-old). Representative μ CT reconstructions of horizontal (left) and vertical (right) views of trabecular bones are shown. (Left, sham-operated, Right, OVX-operated.) **B** Bone structure analysis of the distal metaphyseal femurs of WT ($n = 5$) and OCZF-Tg mice ($n = 4$). Trabecular bone parameters: bone volume per total volume (BV/TV), trabecular thickness (Tb.Th), and trabecular number (Tb.N). **C** Cortical bone structure analysis of the central diaphyseal portions of femurs of WT ($n = 5$) and OCZF-Tg mice ($n = 4$). All data are presented as the mean \pm SD. The statistical differences between mean values were determined by one-way ANOVA followed by Tukey's post hoc test in (B, C). ** $P < 0.01$, * $P < 0.05$.

OVX-induced bone loss was enhanced in OCZF-Tg mice

To know the role of LRF/OCZF in pathological osteolysis *in vivo*, we analyzed the effects of OVX on bone loss in OCZF-Tg mice. In the previous study, peripheral quantitative computed tomography (pQCT) analysis of 6-week-old male femurs showed that OCZF-Tg mice displayed lower BMD and BMC²⁵. In this study, we performed μ CT analysis of trabecular bones of distal femurs from 12-week-old female mice of WT and OCZF-Tg. Bone volume per total volume (BV/TV) of sham-operated OCZF-Tg female mice were significantly lower compared to those of sham-operated WT mice (Fig. 4A, B). In WT mice, OVX-treatment significantly decreased BV/TV and trabecular number compared to those of sham-operated WT mice (Fig. 4A, B). In contrast, OVX-treatment of OCZF-Tg mice markedly decreased not only BV/TV and trabecular number but also trabecular thickness and cortical thickness compared to those of sham-operated OCZF-

Tg mice (Fig. 4B, C). In addition, effects of OVX on BV/TV (-53.5% , $p = 0.0007$ versus sham), trabecular thickness (-14.0% , $p = 0.01$ versus sham), trabecular number (-45.3% , $p = 0.0001$ versus sham), and cortical thickness (-13.7% , $p = 0.001$ versus sham) in OCZF-Tg mice was greater than effects of OVX on BV/TV (-39.1% , $p = 0.0001$ versus sham), trabecular thickness (-6.3% , N.S. versus sham), trabecular number (-33.7% , $p = 0.0003$ versus sham), and cortical thickness (-5.9% , N.S. versus sham) in WT mice (Fig. 4B, C). These results strongly suggest that OCZF overexpression in osteoclasts promotes pathological bone loss *in vivo*.

OCZF overexpression promoted the expression of anti-apoptotic *Bcl-xl*

Anti-apoptotic *Bcl-xl* mRNA and pro-apoptotic *Bcl-xs* mRNA are formed by alternative splicing of *Bcl-x* pre mRNA (Fig. 5A). We first

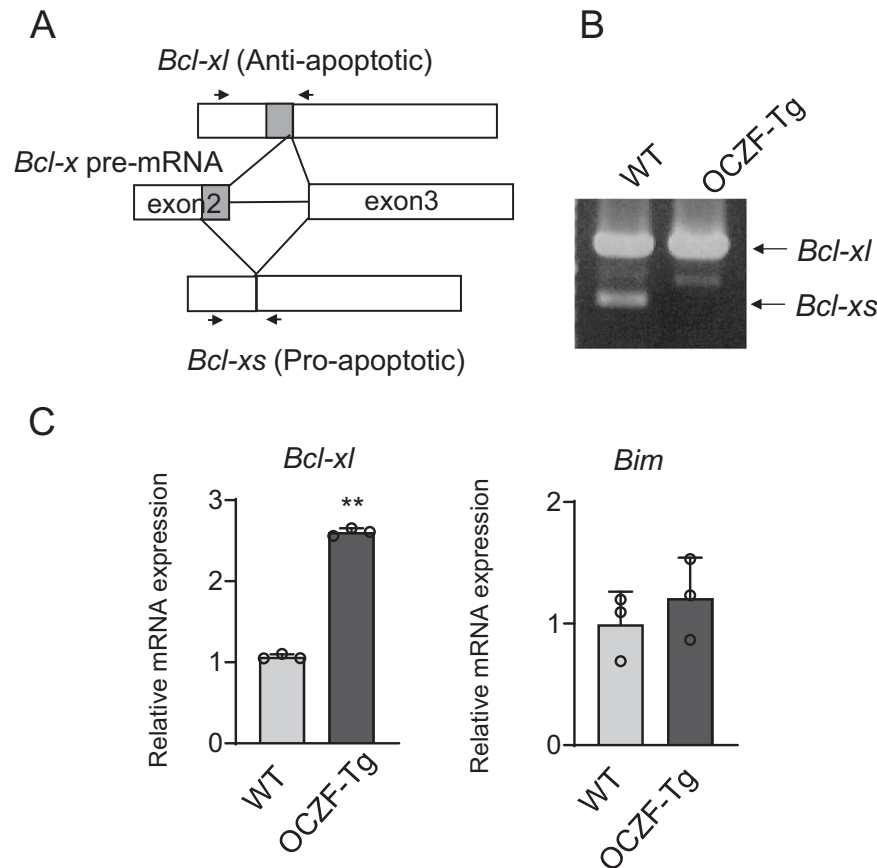


Fig. 5 OCZF overexpression promoted alternative splicing of *Bcl-x* mRNA. **A** Diagram shows alternative splicing from *Bcl-x* pre-mRNA and the formation of *Bcl-xl* (anti-apoptotic) and *Bcl-xs* (pro-apoptotic) mRNA isoforms. Arrows indicate positions of primers used in RT-PCR. **B** RT-PCR analysis of *Bcl-xl* and *Bcl-xs* isoforms at 72 h of culture derived from WT and OCZF-Tg BMMs. **C** RT-qPCR analysis of *Bcl-xl*, and *Bim* expression at 72 h of culture derived from WT and OCZF-Tg BMMs. BMMs cultured with M-CSF (10 ng/ml) and RANKL (50 ng/ml) were harvested at 72 h, and subjected to RT-qPCR. In RT-qPCR analysis, expression was normalized with *Gapdh* ($n = 3$). Data are presented as mean \pm SD. Student's *t*-test was used for statistical analysis. ** $P < 0.01$ compared to the cells of WT mice.

analyzed the expression of *Bcl-x* isoforms in the culture of BMMs stimulated with RANKL. RT-PCR analysis was performed using PCR primers which detect both anti-apoptotic *Bcl-xl* (615 bp) and pro-apoptotic *Bcl-xs* (426 bp) mRNA. Expression of both *Bcl-xl* and *Bcl-xs* isoform mRNAs was detected at 72 h of culture, when osteoclasts are formed from WT BMMs (Fig. 5B). In contrast, expression of *Bcl-xl* but not *Bcl-xs* mRNA was detected at 72 h of culture derived from OCZF-Tg BMMs. To determine the expression of *Bcl-x* mRNA quantitatively, we performed RT-qPCR analysis. *Bcl-xl* isoform mRNA was significantly increased at 72 h of culture derived from OCZF-Tg BMMs compared to that derived from WT BMMs (Fig. 5C). The results suggest that alternative splicing of *Bcl-x* mRNA was suppressed but *Bcl-xl* mRNA alternative splicing was promoted in osteoclasts from OCZF-Tg mice. We also analyzed the expression of *Bim* as a pro-apoptotic gene. The expression of *Bim* in the culture derived from OCZF-Tg BMMs was not significantly changed compared to that derived from WT BMMs (Fig. 5C). The results suggest that OCZF overexpression enhances osteoclast survival by increasing the expression of anti-apoptotic genes.

SAM68 protein level was markedly suppressed in osteoclasts derived from OCZF-Tg mice

Because Sam68 promotes alternative splicing of *Bcl-xs*, and FBI-1 regulates Sam68 activity, we next analyzed whether Sam68 is involved in the function of LRF/OCZF in osteoclasts. We first analyzed the expression of Sam68 in osteoclastogenesis. RT-PCR

analysis showed that *Sam68* mRNA expression was upregulated at 38 h of culture, but down-regulated at 72 h of culture (Fig. 6A). Levels of *Sam68* mRNA at 72 h of culture was not significantly different between WT and OCZF-Tg BMMs. In contrast, Western blot analysis showed SAM68 protein levels were markedly decreased at 72 h of culture derived from OCZF-Tg BMMs (Fig. 6B). Immunostaining of osteoclasts with SAM68 antibody revealed that high expression of SAM68 protein was found in nuclei of mononuclear cells and cytoplasm of osteoclasts derived from WT mice (Fig. 6C and Supplementary Fig. 3). In contrast, fluorescence signals of SAM68 were markedly decreased in OCZF-Tg mice-derived osteoclasts (Fig. 6C and Supplementary Fig. 3). Quantitative analysis of SAM68 fluorescence intensity showed that SAM68 expression was significantly decreased in osteoclasts derived from OCZF-Tg mice compared to that in WT osteoclasts (Fig. 6D), suggesting that OCZF regulates SAM68 protein levels in osteoclasts.

Sam68 knockdown promoted expression of *Bcl-xl* mRNA

Considering the role of SAM68 in alternative splicing of the apoptotic *Bcl-xs* isoform, we analyzed the effect of Sam68 knockdown on the alternative splicing of *Bcl-x* mRNA in the culture of BMMs stimulated with RANKL. Infection of *Sam68* shRNA lentivirus significantly inhibited the expression of *Sam68* mRNA (Fig. 7A). In the infection of control *shEGFP*, expression of *Bcl-xl* and *Bcl-xs* mRNA was detected at 72 h of culture, when osteoclasts are formed (Fig. 7B). In contrast, the expression of *Bcl-xs* mRNA was

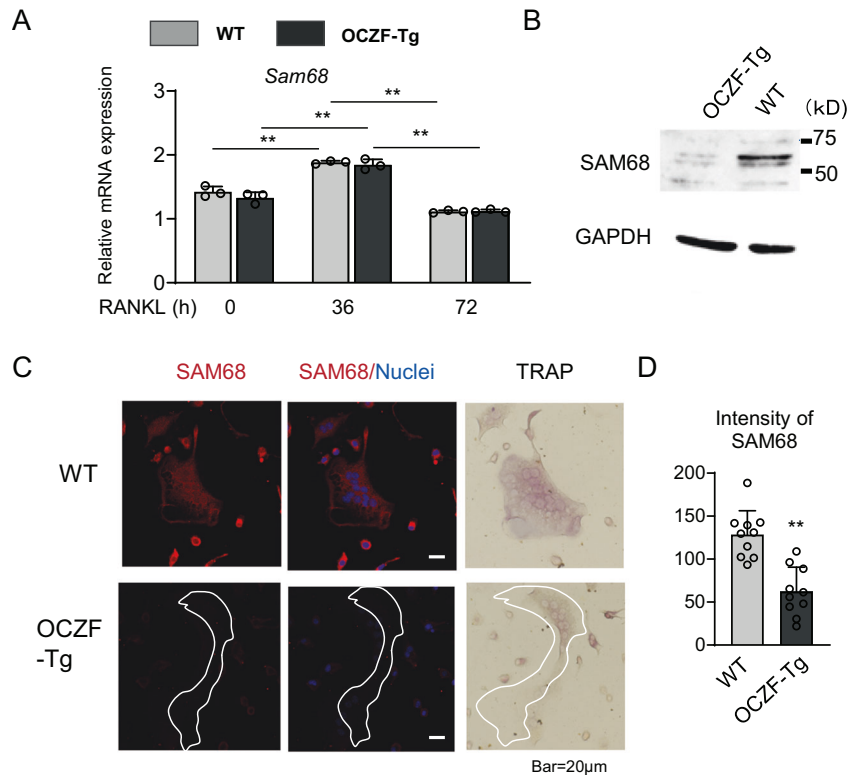


Fig. 6 Expression of SAM68 protein was markedly decreased in OCZF-Tg mice-derived osteoclasts. **A** RT-qPCR analysis for the expression of *Sam68* mRNA in osteoclastogenesis. BMMs cultured with M-CSF (10 ng/ml) and RANKL (50 ng/ml) were harvested at 0, 36, or 72 h, and subjected to RT-qPCR. Expression levels were normalized to that of *Gapdh* ($n = 3$). **B** Western blotting analysis of SAM68 at 72 h of culture derived from WT and OCZF-Tg BMMs. Cell lysates of osteoclasts from WT and OCZF-Tg mice were analyzed. **C** Immunostaining of osteoclasts derived from WT and OCZF-Tg mice. SAM68 (red), Nuclei (blue). TRAP staining was performed after immunostaining. **D** SAM68 protein expression is shown as the average of fluorescence intensity of osteoclasts ($n = 10$). Data are presented as means \pm SD. The differences between means were determined by one-way ANOVA followed by Tukey's post hoc test in **A**. $^{***}P < 0.01$, $^{*}P < 0.05$. Student's *t* test was used for statistical analysis in **(D)**. $^{***}P < 0.01$, compared to the cells of WT mice.

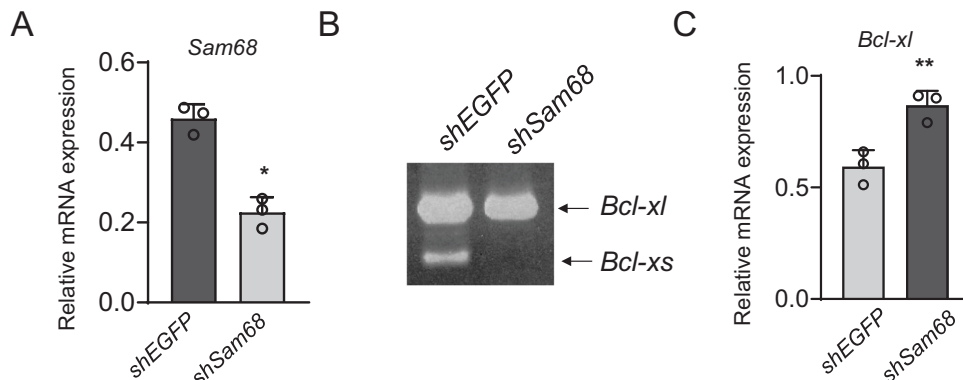


Fig. 7 Sam68 knockdown promoted alternative splicing of *Bcl-xl*. **A** Expression of *Sam68* mRNA in the cells infected with *EGFP* shRNA (control) or *Sam68* shRNA lentivirus. The expression of *Sam68* mRNA was assessed using RT-qPCR. **B** RT-PCR analysis of *Bcl-xl* and *Bcl-xs* isoforms in the cells infected with *shEGFP* or *shSam68*. **C** RT-qPCR analysis of *Bcl-xl* mRNA in the cells infected with *shEGFP* or *shSam68*. BMMs stimulated with RANKL for 48 h were infected with *EGFP* shRNA or *Sam68* shRNA lentivirus. The cells were stimulated with RANKL for another 36 h and the expression of *Sam68*, *Bcl-xl*, or *Bcl-x* isoforms was assessed using RT-qPCR or RT-PCR. In RT-qPCR analysis, expression was normalized with *Gapdh* ($n = 3$). Data are presented as mean \pm SD. Student's *t* test was used for statistical analysis. $^{***}P < 0.01$, $^{*}P < 0.05$ compared to the cells infected with *EGFP* shRNA lentivirus (**A**, **C**).

lost in *shSam68* infected cultures (Fig. 7B). In addition, RT-qPCR analysis showed that the infection of *shSam68* significantly upregulated the expression of *Bcl-xl* mRNA compared to that infected with control *shEGFP* (Fig. 7C). The results suggest that reduction of *Sam68* expression promotes the expression of *Bcl-xl* mRNA and that LRF/OCZF promotes osteoclast survival by down-regulating *Sam68* protein levels.

DISCUSSION

After the osteoclast have completed resorbing bone, osteoclasts die by apoptosis which switches into the bone formation in the process of bone remodeling³⁷. Therefore, the regulation of osteoclast apoptosis is critical to maintain bone remodeling. Inappropriate bone remodeling leads to pathological bone diseases such as osteoporosis and rheumatoid arthritis¹⁶. In this

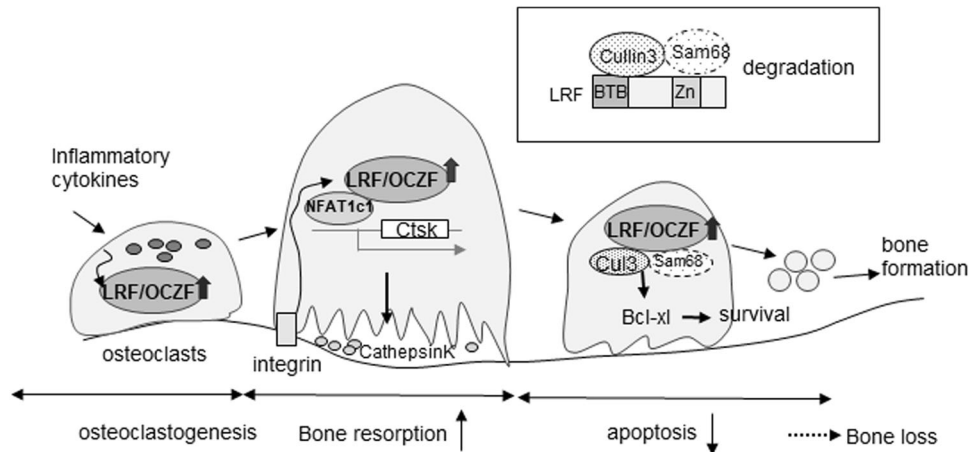


Fig. 8 A possible mechanism of the promotion of bone resorption and osteoclast survival by LRF/OCZF overexpression. In osteoclastogenesis, LRF expression is upregulated by RANKL and inflammatory cytokines, and further increased by integrin signaling. LRF/OCZF enhances the expression of NFATc1 target genes which promotes bone resorption. In osteoclasts, *Bcl-xl* and *Bcl-xs* mRNA are formed by alternative splicing, and RNA binding protein SAM68 mediates *Bcl-xs* alternative splicing. LRF has two conserved domains, the N-terminal BTB domain and the C-terminal zinc finger motifs (shown in framed box). SAM68 binds to zinc finger motifs of LRF, and BTB domain of LRF interacts with CUL3 ubiquitin ligase which leads to the degradation of SAM68 protein. The degradation of SAM68 promotes alternative splicing of *Bcl-xl* and osteoclast survival. Under inflammatory conditions, increased expression of LRF/OCZF may be involved in the pathological bone loss.

study, we show LRF/OCZF which is involved in osteoclast survival is highly expressed in mature osteoclasts and enhances the expression of *Bcl-xl*. LRF/OCZF overexpression in osteoclasts promoted bone loss in OVX-induced mouse model. In addition, we found SAM68-mediated alternative splicing of *Bcl-xl* mRNA is involved in osteoclast survival enhanced by LRF/OCZF. We show a novel mechanism of osteoclast survival regulated by LRF/OCZF-SAM68 axis, and our results strongly suggest that LRF/OCZF is an important target protein to regulate pathological bone resorption.

We previously reported that osteoclast-specific LRF deletion in mice developed increased bone mass phenotype with reduced bone resorption²⁴. We also reported that LRF interacted with NFATc1, and enhanced the expression of several NFATc1 target genes including cathepsin K, which are responsible for bone resorption²⁴. In this study, we analyzed the detailed expression of LRF and colocalization of LRF with NFATc1 in osteoclastogenesis. Consistent with previous results, we found that LRF protein was colocalized with NFATc1 in osteoclast precursor cells and osteoclasts. In addition, LRF expression was correlated with that of cathepsin K in vitro and in vivo. Our results indicate LRF plays a role in osteoclastic bone resorption by enhancing the expression of bone resorption-related genes (Fig. 8). Notably, NFATc1 expression was reduced in several osteoclasts, whereas LRF expression persisted after differentiation into mature osteoclasts, suggesting that LRF/OCZF plays an additional role in bone resorption. LRF expression was enhanced in osteoclasts formed in dentin slices, which are activated by integrin signaling. Src inhibitor altered expression and localization of LRF in osteoclasts. Additionally, FBI-1 has been identified one of genes induced by integrin signaling involved in B cell survival³⁸. It seems that integrin signaling is involved in LRF expression in osteoclasts.

It has been reported that the survival of osteoclasts formed on bone matrix in vitro was enhanced in comparison with those of osteoclasts formed on culture dishes¹⁶. Integrin signaling induces survival signals by increasing the expression of *Bcl-xl* in cancer cells³⁹. In consistent with previous studies, *Bcl-xl* expression was enhanced in osteoclasts formed on dentin slices compared to those formed on culture dishes. Several lines of evidence have shown the important roles of Bcl-2 family proteins in osteoclast apoptosis. Pro-apoptotic Bim is induced in cytokine-deprived osteoclasts and enhanced osteoclast apoptosis, whereas anti-apoptotic Bcl-xl, Bcl-2, and Mcl-2 prolonged osteoclast

survival^{17,18,40,41}. Since it is known that FBI-1 inhibits *Bcl-x* alternative splicing and apoptosis in cancer cells²⁶, we analyzed *Bcl-xl* expression in osteoclasts derived from OCZF-Tg mice. OCZF overexpression enhanced *Bcl-xl* expression which contributed to osteoclast survival. LRF expression is induced by GATA1 in erythropoiesis, and LRF deletion leads to increased apoptosis of late-stage erythroblasts with upregulation of pro-apoptotic factor Bim¹¹. However, LRF/OCZF overexpression did not affect Bim expression in osteoclasts.

Anti-apoptotic *Bcl-x1* isoform and pro-apoptotic *Bcl-x* isoform mRNAs are produced by alternative splicing of *Bcl-x* pre-mRNA (Fig. 5A). Interestingly, we found alternative splicing of *Bcl-x* mRNA was enhanced, whereas alternative splicing of *Bcl-xs* mRNA was decreased in osteoclasts derived from OCZF-Tg mice. FBI-1 regulates *Bcl-x* alternative splicing by regulating the activity of RNA binding protein SAM68²⁶. SAM68 is a member of signal transduction and activator of RNA (STAR) family of RNA binding protein and identified as a specific target of Src tyrosine kinase in mitosis⁴². Sam68 has been identified as regulator of alternative splicing of CD44 and *Bcl-xl*, which are involved in tumor progression and apoptosis⁴³. Sam68 binds to *Bcl-x* mRNA and affects alternative splicing. Sam68 upregulation increased the levels of *Bcl-xs* mRNA, whereas Sam68 depletion caused the accumulation of *Bcl-xl* mRNA, thereby regulates apoptosis²⁷. We found that Sam68 protein levels were markedly decreased in osteoclasts in OCZF-Tg mice, suggesting that OCZF facilitates alternative splicing of *Bcl-xl*. In addition, we confirmed that shRNA-mediated Sam68 inhibition reduced *Bcl-xs* alternative splicing and promoted *Bcl-xl* alternative splicing in osteoclasts. zBTB family proteins is known as an adaptor of CUL3 ubiquitin ligase complexes⁴⁴. It is possible to hypothesize that LRF/OCZF interacts with CUL3 which induces degradation of SAM68 protein. zBTB family proteins have another domains such as zinc finger motifs to recruit substrates of CUL3⁴⁵. Since FBI-1 interacts with SAM68 in the C-terminal region including zinc finger motifs²⁶, BTB domain of LRF/OCZF interacts with CUL3 via BTB domain, which may stimulate the degradation of SAM68 binds to zinc finger domain (Fig. 8). Our results suggest a novel regulatory mechanism of osteoclast survival mediated by LRF/OCZF-SAM68-Bcl-xl (Fig. 8).

To analyze the function of OCZF in osteoclasts, we used OCZF-Tg mice that overexpress OCZF in late stage of osteoclastogenesis. We previously showed that OCZF-Tg male mice exhibited

osteoporotic phenotype²⁵. In this study, we found OCZF-Tg female mice also displayed osteoporotic phenotype. In addition, OCZF overexpression promoted bone loss induced by OVX in mice. The results suggest that overexpression of LRF/OCZF in osteoclasts causes physiological and pathological bone loss in mice. Recent reports show the important roles of osteoclast apoptosis in physiological bone mass and pathological bone loss. 5-Azacytidine-induced protein 2 (AZI2), TNF receptor-associated factor family member-associated NF- κ B activator-binding kinase 1-binding protein regulate bone mass by suppressing Src-mediated osteoclast survival⁴⁶. On the other hands, analysis of in vitro osteoclastogenesis from peripheral blood mononuclear cells showed that osteoclasts derived from patients with active erosive rheumatoid arthritis displayed resistant to apoptosis^{47,48}. Targeted delivery of cytotoxic chemotherapeutic drug to induce apoptosis of osteoclasts suppressed bone destruction in arthritic joints of arthritis rats⁴⁹. In addition, estrogen deficiency altered the expression of gene which is involved osteoclast apoptosis⁵⁰. Thus, the regulation of osteoclast apoptosis is important to control not only inflammatory bone destruction but also osteoporotic bone loss. However, adenovirus-mediated *Bcl-xl* overexpression prolonged osteoclast survival but reduced bone resorption, and osteoclast-specific *Bcl-xl* deletion in mice displayed decreased bone mass phenotype¹⁸. It seems that only enhanced expression of *Bcl-xl* by LRF/OCZF may not be responsible for bone loss. However, a recent analysis of LRF binding promoter sequences revealed that LRF affects transcription of a wide range of genes⁵¹. It is possible that OCZF overexpression may affect the suppressive effect of *Bcl-xl* on bone resorption. Interestingly, LRF collaborates with transcriptional factor p65 to modify the accessibility of gene transcription regulatory regions to secondary transcriptional factors, thereby influences multiple genes⁵¹. Since LRF/OCZF expression is augmented by inflammatory cytokines, our results suggest that enhanced LRF/OCZF expression may contributes to bone destruction under inflammatory conditions.

In conclusion, we have shown LRF/OCZF expression is associated with osteoclast survival, and LRF/OCZF overexpression causes bone loss and also markedly promotes OVX-induced bone loss. LRF/OCZF overexpression enhanced osteoclast survival by regulating SAM68-mediated alternative splicing of *Bcl-xl* mRNA. Our findings show a novel mechanism of osteoclast survival regulated by zBTB family protein LRF/OCZF and RNA-binding protein SAM68. Our results suggest that LRF/OCZF induced by inflammatory cytokines play an important role in pathological bone loss, and the current study provides a novel insight into the development of therapeutic drugs to treat pathological bone diseases.

DATA AVAILABILITY

All data generated or analyzed during this study are included in this published article.

REFERENCES

1. Maeda T. Regulation of hematopoietic development by ZBTB transcription factors. *Int J Hematol* **104**, 310–323 (2016).
2. Gupta S, Singh AK, Prajapati KS, Kushwaha PP, Shuaib M, Kumar S. Emerging role of ZBTB7A as an oncogenic driver and transcriptional repressor. *Cancer Lett* **483**, 22–34 (2020).
3. Constantinou C, Spella M, Chondrou V, Patrinos GP, Papachatzopoulou A, Sgourou A. The multi-faceted functioning portrait of LRF/ZBTB7A. *Hum Genomics* **13**, 66 (2019).
4. Singh AK, Verma, Kushwaha PP, Prajapati KS, Shuaib M, Kumar S, et al. Role of ZBTB7A zinc finger in tumorigenesis and metastasis. *Mol Biol Rep.* <https://doi.org/10.1007/s11033-021-06405-x> (2021).
5. Wang G, Lunardi A, Zhang J, Chen Z, Ala U, Webster KA, et al. Zbtb7a suppresses prostate cancer through repression of a Sox9-dependent pathway for cellular senescence bypass and tumor invasion. *Nat Genet* **45**, 739–746 (2013).

6. Lunardi A, Guarnerio J, Wang G, Maeda T, Pandolfi PP. Role of LRF/Pokemon in lineage fate decisions. *Blood* **121**, 2845–2853 (2013).
7. Lee SU, Maeda T. POK/ZBTB proteins: An emerging family of proteins that regulate lymphoid development and function. *Immunol Rev* **247**, 107–119 (2012).
8. Maeda T, Merghoub T, Hobbs RM, Dong L, Maeda M, Zakrzewski J, et al. Regulation of B versus T lymphoid lineage fate decision by the proto-oncogene LRF. *Science* **316**, 860–866 (2007).
9. Vacchio MS, Wang L, Bouladoux N, Carpenter AC, Xiong Y, Williams LC, et al. A ThPOK-LRF transcriptional node maintains the integrity and effector potential of post-thymic CD4+ T cells. *Nat Immunol* **15**, 947–956 (2014).
10. Sakurai N, Maeda M, Lee SU, Ishikawa Y, Li M, Williams JC, et al. The LRF transcription factor regulates mature B cell development and the germinal center response in mice. *J Clin Invest* **121**, 2583–2598 (2011).
11. Maeda T, Ito K, Merghoub T, Polisen L, Hobbs RM, Wang G, et al. LRF is an essential downstream target of GATA1 in erythroid development and regulates BIM-dependent apoptosis. *Dev Cell* **17**, 527–540 (2009).
12. Xu L, Wei Y, Reboul J, Vaglio P, Shin TH, Vidal M, et al. BTB proteins are substrate-specific adaptors in an SCF-like modular ubiquitin ligase containing CUL-3. *Nature* **425**, 316–321 (2003).
13. Mathew R, Seiler MP, Scanlon ST, Mao AP, Constantinides MG, Bertozzi-Villa C, et al. BTB-ZF factors recruit the E3 ligase cullin 3 to regulate lymphoid effector programs. *Nature* **491**, 618–621 (2012).
14. Jimi E, Nakayama I, Ikebe T, Akiyama S, Takahashi N, Suda T. Activation of NF- κ B is involved in the survival of osteoclasts promoted by interleukin-1. *J Biol Chem* **273**, 8799–8805 (1998).
15. Lee SE, Chung WJ, Kwak HB, Chung CH, Kwack KB, Lee ZH, et al. Tumor necrosis factor- α supports the survival of osteoclasts through the activation of Akt and ERK. *J Biol Chem* **276**, 49343–49349 (2001).
16. Soysa NS, Alles N. Positive and negative regulators of osteoclast apoptosis. *Bone Rep* **11**, 100225 (2019).
17. Nagase Y, Iwasawa M, Akiyama T, Kadono Y, Nakamura M, Oshima Y, et al. Anti-apoptotic molecule Bcl-2 regulates the differentiation, activation, and survival of both osteoblasts and osteoclasts. *J Biol Chem* **284**, 36659–36669 (2009).
18. Iwasawa M, Miyazaki T, Nagase Y, Akiyama T, Kadono Y, Nakamura M, et al. The antiapoptotic protein Bcl-xL negatively regulates the bone-resorbing activity of osteoclasts in mice. *J Clin Invest* **119**, 3149–3159 (2009).
19. Ding N, Liu C, Yao L, Bai Y, Cheng P, Li Z, et al. Alendronate induces osteoclast precursor apoptosis via peroxisomal dysfunction mediated ER stress. *J Cell Physiol* **233**, 7415–7423 (2018).
20. Zhang Q, Badell IR, Schwarz EM, Boulukos KE, Yao Z, Boyce BF, et al. Tumor necrosis factor prevents alendronate-induced osteoclast apoptosis in vivo by stimulating Bcl-xL expression through Ets-2. *Arthritis Rheum* **52**, 2708–2718 (2005).
21. Nakamura T, Imai Y, Matsumoto T, Sato S, Takeuchi K, Igarashi K, et al. Estrogen prevents bone loss via estrogen receptor alpha and induction of Fas ligand in osteoclasts. *Cell* **130**, 811–823 (2007).
22. Kim HN, Ponte F, Nookaew I, Ucer Ozgurel S, Marques-Carvalho A, Iyer S, et al. Estrogens decrease osteoclast number by attenuating mitochondria oxidative phosphorylation and ATP production in early osteoclast precursors. *Sci Rep* **10**, 11933 (2020).
23. Fischer V, Haffner-Luntzer M. Interaction between bone and immune cells: Implications for postmenopausal osteoporosis. *Semin Cell Dev Biol.* <https://doi.org/10.1016/j.semcdb.2021.05.014> (2021).
24. Tsuji-Takechi K, Negishi-Koga T, Sumiya E, Kukita A, Kato S, Maeda T, et al. Stage-specific functions of leukemia/lymphoma-related factor (LRF) in the transcriptional control of osteoclast development. *Proc Natl Acad Sci USA* **109**, 2561–2566 (2012).
25. Kukita A, Kukita T, Nagata K, Teramachi J, Li YJ, Yoshida H, et al. The transcription factor FBI-1/OCZF/LRF is expressed in osteoclasts and regulates RANKL-induced osteoclast formation in vitro and in vivo. *Arthritis Rheum* **63**, 2744–2754 (2011).
26. Bielli P, Busa R, Di Stasi SM, Munoz MJ, Botti F, Kornbliht AR, et al. The transcription factor FBI-1 inhibits SAM68-mediated BCL-X alternative splicing and apoptosis. *EMBO Rep* **15**, 419–427 (2014).
27. Paronetto MP, Achsel T, Massiello A, Chalfant CE, Sette C. The RNA-binding protein Sam68 modulates the alternative splicing of Bcl-x. *J Cell Biol* **176**, 929–939 (2007).
28. Taylor SJ, Shalloway D. An RNA-binding protein associated with Src through its SH2 and SH3 domains in mitosis. *Nature* **368**, 867–871 (1994).
29. Gaytan-Cervantes J, Gonzalez-Torres C, Maldonado V, Zampedi C, Ceballos-Cancino G, Melendez-Zajgla J. Protein Sam68 regulates the alternative splicing of survivin DEx3. *J Biol Chem* **292**, 13745–13757 (2017).
30. Xu X, Hirata H, Shiraki M, Kamohara A, Nishioka K, Miyamoto H, et al. Prostate transmembrane protein androgen induced 1 is induced by activation of osteoclasts and regulates bone resorption. *FASEB J* **33**, 4365–4375 (2019).

31. Funakubo N, Xu X, Kukita T, Nakamura S, Miyamoto H, Kukita A. Pmepa1 induced by RANKL-p38 MAPK pathway has a novel role in osteoclastogenesis. *J Cell Physiol* **233**, 3105–3118 (2018).
32. Zhang JQ, Takahashi A, Gu JY, Zhang X, Kyumoto-Nakamura Y, Kukita A, et al. In vitro and in vivo detection of tunneling nanotubes in normal and pathological osteoclastogenesis involving osteoclast fusion. *Lab Invest.* <https://doi.org/10.1038/s41374-021-00656-9> (2021).
33. Shiraki M, Xu X, Iovanna JL, Kukita T, Hirata H, Kamohara A, et al. Deficiency of stress-associated gene Nupr1 increases bone volume by attenuating differentiation of osteoclasts and enhancing differentiation of osteoblasts. *FASEB J* **33**, 8836–8852 (2019).
34. Miyazaki T, Sanjay A, Neff L, Tanaka S, Horne WC, Baran R. Src kinase activity is essential for osteoclast function. *J Biol Chem* **279**, 17660–17666 (2004).
35. Gingery A, Bradley E, Shaw A, Oursler MJ. Phosphatidylinositol 3-kinase coordinately activates the MEK/ERK and AKT/NFkappaB pathways to maintain osteoclast survival. *J Cell Biochem* **89**, 165–179 (2003).
36. Hussein O, Tiedemann K, Komarova SV. Breast cancer cells inhibit spontaneous and bisphosphonate-induced osteoclast apoptosis. *Bone* **48**, 202–211 (2011).
37. Henriksen K, Neutzsky-Wulff AV, Bonewald LF, Karsdal MA. Local communication on and within bone controls bone remodeling. *Bone* **44**, 1026–1033 (2009).
38. Astier AL, Xu R, Svoboda M, Hinds E, Munoz O, de Beaumont R, et al. Temporal gene expression profile of human precursor B leukemia cells induced by adhesion receptor: identification of pathways regulating B-cell survival. *Blood* **101**, 1118–1127 (2003).
39. Lamb LE, Zarif JC, Miranti CK. The androgen receptor induces integrin alpha6beta1 to promote prostate tumor cell survival via NF-kappaB and Bcl-xL. Independently of PI3K signaling. *Cancer Res* **71**, 2739–2749 (2011).
40. Masuda H, Hirose J, Omata Y, Tokuyama N, Yasui T, Kadono Y, et al. Anti-apoptotic Bcl-2 family member Mcl-1 regulates cell viability and bone-resorbing activity of osteoclasts. *Bone* **58**, 1–10 (2014).
41. Akiyama T, Bouillet P, Miyazaki T, Kadono Y, Chikuda H, Chung UI, et al. Regulation of osteoclast apoptosis by ubiquitylation of proapoptotic BH3-only Bcl-2 family member Bim. *EMBO J* **22**, 6653–6664 (2003).
42. Fumagalli S, Totty NF, Hsuan JJ, Courtneidge SA. A target for Src in mitosis. *Nature* **368**, 871–874 (1994).
43. Meyer NH, Tripsianes K, Vincendeau M, Madl T, Kateb F, Brack-Werner R, et al. Structural basis for homodimerization of the Src-associated during mitosis, 68 kDa protein (Sam68) Qua1 domain. *J Biol Chem* **285**, 28893–28901 (2010).
44. Geyer R, Wee S, Anderson S, Yates J, Wolf DA. BTB/POZ domain proteins are putative substrate adaptors for cullin 3 ubiquitin ligases. *Mol Cell* **12**, 783–790 (2003).
45. Chen HY, Chen RH. Cullin 3 ubiquitin ligases in cancer biology: Functions and therapeutic implications. *Front Oncol* **6**, 113 (2016).
46. Maruyama K, Fukasaka M, Uematsu S, Takeuchi O, Kondo T, Saitoh T, et al. 5-Azacytidine-induced protein 2 (AZI2) regulates bone mass by fine-tuning osteoclast survival. *J Biol Chem* **290**, 9377–9386 (2015).
47. Durand M, Boire G, Komarova SV, Dixon SJ, Sims SM, Harrison RE, et al. The increased in vitro osteoclastogenesis in patients with rheumatoid arthritis is due to increased percentage of precursors and decreased apoptosis—the In Vitro Osteoclast Differentiation in Arthritis (IODA) study. *Bone* **48**, 588–596 (2011).
48. Allard-Chamard H, Carrier N, Dufont P, Durand M, de Brum-Fernandes AJ, Boire G, et al. Osteoclasts and their circulating precursors in rheumatoid arthritis: Relationships with disease activity and bone erosions. *Bone Rep* **12**, 100282 (2020).
49. Deng C, Zhang Q, He P, Zhou B, He K, Sun X, et al. Targeted apoptosis of macrophages and osteoclasts in arthritic joints is effective against advanced inflammatory arthritis. *Nat Commun* **12**, 2174 (2021).
50. Zhang B, Yuan P, Xu G, Chen Z, Li Z, Ye H, et al. DUSP6 expression is associated with osteoporosis through the regulation of osteoclast differentiation via ERK2/Smad2 signaling. *Cell Death Dis* **12**, 825 (2021).
51. Ramos Pittol JM, Oruba A, Mittler G, Sacconi S, van Essen D. Zbtb7a is a transducer for the control of promoter accessibility by NF-kappa B and multiple other transcription factors. *PLoS Biol* **16**, e2004526 (2018).

ACKNOWLEDGEMENTS

This work was supported in part by JSPS KAKENHI Grant Numbers JP 15K11046 and 18K09034.

AUTHOR CONTRIBUTIONS

X.X. and A.K. (Kukita), designed, performed experiments, and analyzed the data; T.S. and M.M. (Murayama), maintained OCZF-Tg mice; X.X., M.S., A.K. (Kamohara), and H.H. prepared OVX mice. D.M. and M.U. performed statistical analysis; T.K. performed immunostaining of bone specimen of arthritis rats; T.M. and M.M. (Mawatari) provided useful discussion. A.K. (Kukita) wrote the manuscript.

COMPETING INTERESTS

The authors declare no competing interests.

ETHICS APPROVAL AND CONSENT TO PARTICIPATE

All experiments were carried out according to the protocol approved by the Laboratory Animal Care and Use Committee of Saga University and Kyushu University. All authors read and approved the final paper.

ADDITIONAL INFORMATION

Supplementary information The online version contains supplementary material available at <https://doi.org/10.1038/s41374-022-00792-w>.

Correspondence and requests for materials should be addressed to Akiko Kukita.

Reprints and permission information is available at <http://www.nature.com/reprints>

Publisher's note Springer Nature remains neutral with regard to jurisdictional claims in published maps and institutional affiliations.